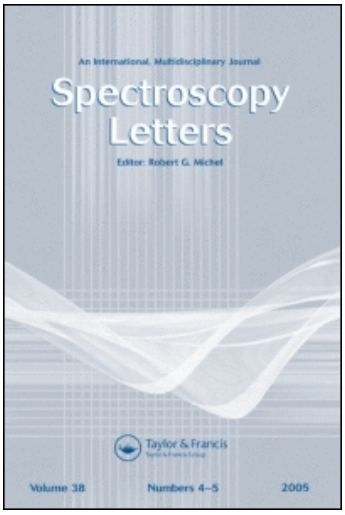

Spectroscopy Letters
Publication details, including instructions for authors and subscription information:
http://www.informaworld.com/smpp/title~content=t713597299

Energy Transfer Processes in Highly Rare-Earth-Doped Planar YAG Waveguides

M. Malinowski[ab]; M. Nakielska[ab]; R. Piramidowicz[a]; J. Sarnecki[b]
[a] Institute of Microelectronics and Optoelectronics PW, Warsaw, Poland [b] Institute of Electronic Materials Technology, Warsaw, Poland

To cite this Article Malinowski, M. , Nakielska, M. , Piramidowicz, R. and Sarnecki, J.(2007) 'Energy Transfer Processes in Highly Rare-Earth-Doped Planar YAG Waveguides', Spectroscopy Letters, 40: 2, 271 — 292
To link to this Article: DOI: 10.1080/00387010701247423
URL: http://dx.doi.org/10.1080/00387010701247423

Spectroscopy Letters, 40: 271–292, 2007

ISSN 0038-7010 print/1532-2289 online
DOI: 10.1080/00387010701247423

Energy Transfer Processes in Highly Rare-Earth–Doped Planar YAG Waveguides

M. Malinowski and M. Nakielska
Institute of Microelectronics and Optoelectronics PW, Warsaw, Poland and Institute of Electronic Materials Technology, Warsaw, Poland

R. Piramidowicz
Institute of Microelectronics and Optoelectronics PW, Warsaw, Poland

J. Sarnecki
Institute of Electronic Materials Technology, Warsaw, Poland

Abstract: We report on the concentration effects on active ion emissions in planar waveguides of YAG:RE^{3+} (RE = Nd, Yb, and Pr) obtained by liquid phase epitaxy on YAG substrates. Liquid phase epitaxy method, which in contrast to the standard Czochralski crystal growth technique, allowed high concentrations of activator, up to 10 at. %, to be obtained. We have investigated emission spectra, the dynamics of the emitting states and the transition linewidths in a wide concentration range. The cross-relaxation and up-conversion transfer rates dependence on concentration was determined.

Keywords: Cross-relaxation, energy transfer, planar waveguide, rare-earth–doped YAG, upconversion

Received 31 May 2006, Accepted 24 August 2006.

The authors were invited to contribute this paper to a special issue of the journal entitled "Spectroscopy of Lanthanide Materials." This special issue was organized by Professor Peter Tanner, City University of Hong Kong, Kowloon.

Address correspondence to M. Malinowski, Institute of Microelectronics and Optoelectronics PW, a ul. Koszykowa 75, 00-662, Warsaw, Poland. E-mail: m.malinowski@elka.pw.edu.pl

INTRODUCTION

Recent attempts to improve the characteristics of waveguide-type and thin disk lasers lead to the use of highly concentrated active media. These lasers are considered as promising systems due to their ability for low threshold, high gain per unit pumping power, high stability, and capability of easy integration with other optical components. Waveguides appear also to be most suitable for nonlinear effects such as frequency doubling and upconversion. The most well-known matrix for such systems are single crystals of $Y_3Al_5O_{12}$ garnet (YAG) doped with Nd^{3+}, Yb^{3+}, or other RE^{3+} ions.[1–5] Highly RE^{3+}-doped YAG crystals are also promising as an efficient, high-power microchip laser material.[6] The high concentration of activator in YAG brings problems of the decrease of the emission quantum efficiency due to self-quenching by cross-relaxation, upconversion, and diffusion mechanisms. Investigation of these processes is important to better understand the interaction between the active centers that determine the desired characteristics of a laser device.

The maximum concentration of RE ions like Nd^{3+} or Pr^{3+} in bulk YAG crystals, obtained using the standard Czochralski method, is limited to about 2 at.%.[7] Thus, the spectroscopic data on concentration effects in these systems are limited to narrow concentration range by the availability of the appropriate samples. Highly doped RE:YAG films could be produced by liquid phase epitaxy technique (LPE).[1] In the LPE from the melt, in the presence of an excess of PbF_2–PbO flux, much higher concentrations, up to about 10 at.% of neodymium or praseodymium, in YAG could be obtained. This was first confirmed by the reports of Hooge[8] who obtained highly concentrated Pr:YAG crystals by flux-growing method.

Guy et al.[9] reported on the investigation of upconversion effects in Nd:YAG LPE films for different doping levels, 1–6 at.% Nd^{3+}, and showed its importance in reduction of the small-signal gain. Recently Mao et al.[10] studied the dependence of the lifetime of highly doped Nd:YAG crystals on temperature. Although there has been significant research on the spectroscopic and laser characterization of Pr^{3+} in single crystals of YAG,[11,12] no work to our knowledge has been performed on Pr^{3+} in crystalline YAG waveguides.

The motivation for this work was to further our knowledge of the effects of energy transfer in RE^{3+}:YAG planar waveguides over the large range of activator concentration and to study the influence of concentration on their emissions.

MATERIALS AND METHODS

The LPE technique was used for growing RE:YAG/YAG epitaxial optical waveguide structures at the Institute of Electronic Materials Technology (ITME) in Warsaw. The layers were grown from a supercooled molten garnet flux ($PbO–B_2O_3$) high-temperature solution.[13] Epitaxy was carried out at

<111> oriented, 20-mm diameter, undoped substrates. The thickness of films varied from about 2 to 20 μm. The creation of active YAG waveguide on YAG substrate requires an increase of refractive index difference between epitaxial layer and a substrate. For this purpose, the substitution of aluminum by gallium ions (Ga^{3+}) was employed. The introduction of large concentration of activator and gallium into the film causes a necessity of lattice mismatch compensation with a small optically inert ion like lutetium (Lu^{3+}) in yttrium sites. Thus, the composition of obtained waveguide films could be described as $Y_{3-x-y}RE_xLu_yAl_{5-z}Ga_zO_{12}$. The highest obtained concentration of neodymium and praseodymium in YAG films was about 10 at.% when Yb^{3+}:YAG films were doped up to 15%. The rectangular ($1 \times 5 \times 8\ mm^3$) samples were cut and polished at end faces for optical measurements.

Polarized absorption measurements in the range 300–700 nm were made using a Cary 2300 Varian spectrometer (Varian, Inc., Palo Alto, CA, USA) equipped with a continuous-flow helium cryostat. Fluorescence and excitation spectra were obtained using a Continuum ND60 (Excel Technology, NY, USA) or Spectra 380 (Spectra-Physics, CA, USA) tunable laser, operating with various dyes, pumped by a frequency doubled Continuum Surelite I Nd:YAG laser (10 ns pulse length, 10 Hz repetition rate, and 180 mJ energy per pulse at 532 nm) or by continuous wave Coherent Innova 300, 10 W argon ion laser, respectively. For excitation in the IR region, the output wavelength of a tunable dye laser was 4155 cm^{-1} downshifted by stimulated Raman scattering (SRS) in a gaseous H_2 cell. In part of the experiments, an argon laser (Coherent Innova 300) pumped sapphire–Ti laser (Coherent 890 Ring Laser), tunable from 730 nm to 990 nm, was the excitation source. The spectra were recorded using a 1-m monochromator with dispersion of 8 Å/mm and detected by Thorn EMI 9789 or RCA C 31034-02 cooled AsGa photomultiplier. Data acquisition was obtained with a Stanford SR 4000 (Stanford Research System) boxcar averager controlled with a PC computer. Fluorescence lifetime measurements were made using a Stanford SR430 multichannel analyzer. The best temporal resolution of the experimental apparatus is 5 ns. To minimize the effect of reabsorption, the fluorescence was excited in the front-face excitation geometry, and the lifetime measurements were made on the nonresonant 1.064-μm lines where the effect of reabsorption will be negligible. Sample cooling was provided by a closed-cycle He optical cryostat, which allowed the temperature to be varied between 10 and 300 K.

The growth of high-quality garnet epitaxial layers is limited by lattice mismatch between the film and substrate. Diffraction measurements were performed using X-ray quasi-parallel double-crystal arrangement with 400 reflection on a Ge monochromator and 444 YAG reflection of CuK_{a1} radiation.[13] For film and substrate lattice deference, two peaks appear in the XRD rocking curve. In the case of good film lattice match to the substrate, obtained for example for $Y_{2,97}$-$yNd_{0,03}Lu_yAl_{5-z}Ga_zO_{12}$/YAG/YAG structure, the recorded XRD patterns indicate one single peak (Fig. 1).

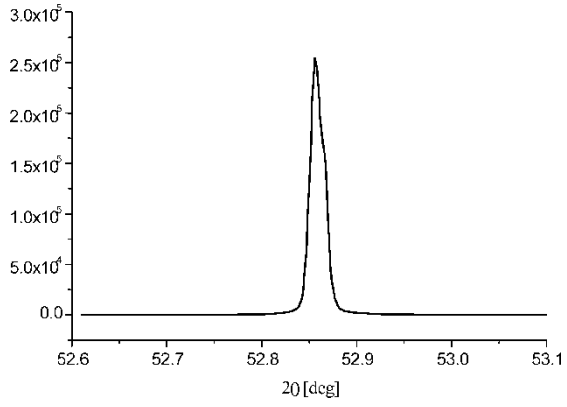

Figure 1. Rocking curves for the lattice matched films of Nd + Lu + Ga:YAG deposited by LPE on YAG substrate.

RESULTS AND DISCUSSION

Nd:YAG

In our experiments, we used excitation into the $^4F_{3/2}$ multiplet of the Nd^{3+} ion and registered emissions centered at 0.9 μm and 1.064 μm corresponding with the $^4F_{3/2} \rightarrow {}^4I_{9/2}$ and $^4I_{11/2}$ transitions, respectively. These investigations were performed under low excitation intensities to prevent the effects of depletion of the ground state and upconversion.

Emission spectra recorded at room temperature showed the same features as reported for Nd^{3+}:YAG bulk samples. Figure 2 shows low-temperature excitation spectra in the region of the lower Stark component of the $^4F_{3/2}$ state (at 11,426 cm^{-1}) of Nd^{3+} ion in YAG. The laser was tuned through the $^4I_{9/1}(1) \rightarrow {}^4F_{3/2}(1)$ absorption line, and total emission around 1.064 μm was registered. The spectra were measured for low-concentration sample containing 1 at.% of Nd^{3+} ions, which is a typical activation level of bulk laser crystals, and for the high concentration waveguide with Nd^{3+} concentration of 6 at.%. In 6 at.% doped sample, the optical linewidth FWHM (full width at half maximum) was 3.2 cm^{-1} and was larger than 0.7 cm^{-1} determined for 1 at.% Nd^{3+} sample. As can be seen in Figure 2, in the vicinity of the main transition there is additional line structure. In highly concentrated sample, the structure of satellites is less resolved, but intensities of lines ABC with respect to the central transition are enhanced. At higher temperatures, the spectral resolution is lost, and additional transitions contribute to an inhomogeneous broadening of the whole transition. This structure, revealed by high-resolution spectroscopy, indicates the presence of several different structural centers. It is interesting to note that the number of additional lines, their relative intensities and spectral positions is similar to

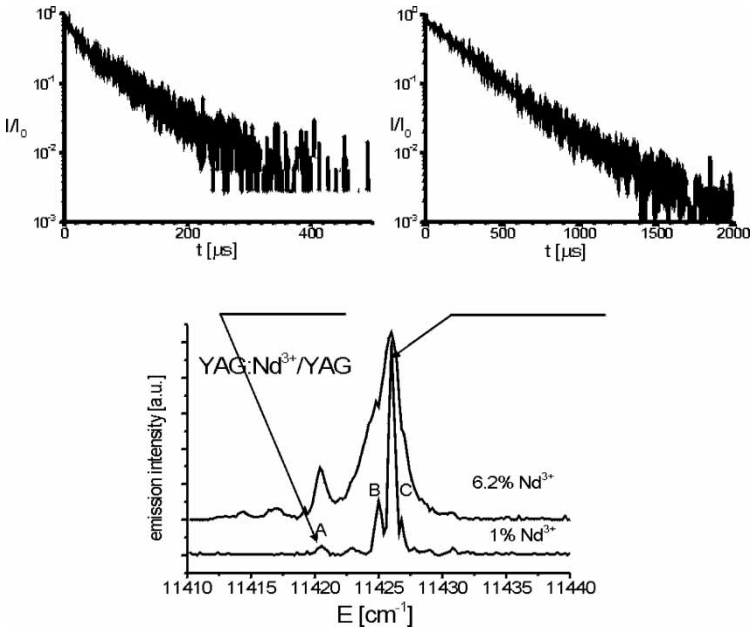

Figure 2. Excitation spectra of the 1064-nm $^4F_{3/2}$ emission in the vicinity of the lowest Stark component of the $^4F_{3/2}$ manifold at 875.2 nm (11,426 cm^{-1}). Selectively excited fluorescence decays of the $^4F_{3/2}$ emission are shown in the upper part of the figure; T = 10 K.

those observed in Nd:YAG single crystals, ceramics, and crystals grown by the TGT (temperature gradient technique) method.[10,14,15] This confirms that the Nd:YAG waveguides grown by the LPE method have no additional defects and are of high quality. The satellite levels could be ascribed to ion pairs for which each peak represents one type of ion-pair lattice configuration. An assignment of satellite lines has been proposed by Lupei [14] who associated line A in Figure 2 with first neighbor and lines B and C with second neighbor neodymium ion pairs.

The decay profiles of the nonresonant $^4F_{3/2} \rightarrow {}^4I_{11/2}$ luminescence were measured after pulse excitation into $^4F_{3/2}$ level. Decay of 1 at.% Nd:YAG measured at room temperature, which is shown in Figure 3, is quasi-exponential with the decay time of 259 μs. At room temperature, when the Nd^{3+} concentration increases, a shortening of the decays is observed. Samples with high neodymium concentration show also nonexponentiality of the decay (Fig. 3). In the case of departure from exponential decay, effective lifetimes τ_{eff} were calculated by numerical integration of the measured decay curve as

$$\tau_{eff} = \int_0^\infty I(t)dt/I(0) \tag{1}$$

where $I(t)$ is the fluorescence intensity emitted from the level.

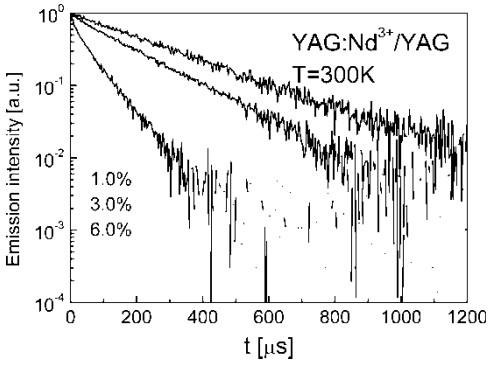

Figure 3. $^4F_{3/2}$ emission decays of Nd^{3+}:YAG epitaxial waveguides for different activator concentrations; T = 300 K.

It is recognized that in Nd^{3+}:YAG, the $^4F_{3/2}$ measured fluorescence lifetime can vary within some range depending on the method of crystal fabrication and the excitation conditions. The values ranging from about 230 μs to 420 μs for polycrystalline sample of 0.01% Nd^{3+} YAG were reported.[16] When such polycrystals were either fused or used to pull single crystals from the melt, the fluorescence lifetime was reduced to about 280 μs. Fluorescence lifetime values of 260 μs and 270 μs were reported by Lupei et al.[17,18] for 0.1% Nd^{3+}:YAG crystal at room and 4.2 K temperatures, respectively. These lifetime values agree with the radiative lifetime computed by Krupke [19] of 259 ± 25 μs or the 272 μs given by Devor et al.[20] As Nd^{3+} in gallium and lutetium garnets exhibits fluorescence lifetime of 270 μs,[21] it could be supposed that in the Nd + Lu + Ga:YAG waveguides the $^4F_{3/2}$ lifetime could be slightly modified with respect to singly doped Nd:YAG.

In Nd:YAG, the multiphonon emission from the $^4F_{3/2}$ level is negligible,[22] and the nonradiative transition rate is dominantly determined by the energy transfer rate. Thus concentration quenching rates are described by the expression $X = 1/\tau_{eff} - 1/\tau_0$, where τ_0 is the $^4F_{3/2}$ lifetime at very low activator concentrations, which value is $\tau_0 \approx 270$ μs. The dependence of the lifetime and the quenching rate on concentration is shown in Figure 4, together with our experimental data for 0.1, 0.5, 0.9, and 1.5 at.% Nd^{3+} bulk YAG crystals.

It is recognized that in Nd^{3+}:YAG at low pump intensities, the concentration-dependent quenching mechanism is related to the energy transfer cross-relaxation of the type $^4F_{3/2} + {}^4I_{9/2} \rightarrow {}^4I_{15/2} + {}^4I_{15/2} \rightarrow {}^4I_{9/2} + {}^4I_{9/2}$.[18] This ion pair process was studied by analyzing decay profiles of the $^4F_{3/2}$ neodymium fluorescence under selective excitation at 10 K of the central line and the satellites as shown in the upper part of Figure 2. In these experiments, we excited selectively into the inhomogeneous profile of the $^4I_{9/2} \rightarrow {}^4F_{3/2}$ absorption and registered total IR emission resulting from the $^4F_{3/2} \rightarrow {}^4I_{11/2}$

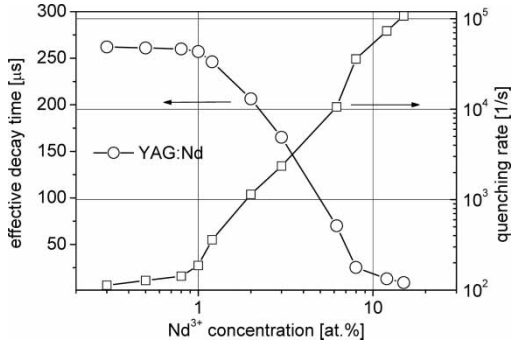

Figure 4. Lifetimes of the $^4F_{3/2}$ level and the cross-relaxation rates in Nd^{3+}:YAG epitaxial waveguides as function of Nd^{3+} concentration.

transition. Thus, due to the partial superposition of the absorption and emission spectra resulting from different structural centers, the resolution of emissions is not perfect. Decay measured after selective excitation of the main line is shown over a large time interval of 2000 μs. Beginning of this decay, up to about 1000 μs, is exponential with the lifetime similar to that measured at 300 K. From the small deviation from a straight-line behavior at late times, the isolated Nd^{3+} ions decay of about 270 μs can be subtracted. When the satellite A was pumped, the emission decay was faster than after excitation of the line center and nonexponential at an early time. Assuming that the pair lifetime reduction is due to cross-relaxation between an excited and unexcited Nd^{3+} ion, the cross-relaxation rate X_A of the satellite A is found to be $5.5 \times 10^4\ s^{-1}$. This value is higher than that reported for Nd^{3+}-doped $LiYF_4$[23] where $X_{01} = 9.9 \times 10^3\ s^{-1}$ but is close to the estimated dipolar contribution to the nearest acceptors transfer for Nd:YAG [24] of $7.5 \times 10^4\ s^{-1}$.

In our studies of the fluorescence dynamics after resonant excitation into the $^4F_{3/2}$ level, we did not observe very fast initial decay, of the order 1 μs, reported by Lupei[14,24] after non resonant excitation at 532 nm and used as an evidence of short-range superexchange interaction.

In the case where each Nd^{3+} ion sees the same environment and assuming the direct interaction for all neodymium pairs and the transfer rate dependence only on the distance, the global transfer rate can be described as a sum over all possible positions of acceptors, which for the dipole–dipole interaction has the form

$$X = X_{01} C_A \sum_{i=1} n_i \left(\frac{R_{01}}{R_{0i}} \right)^6 \tag{2}$$

where $X_{01} = X_A$ is the nearest neighbor trapping rate, n_i is the coordination number of ion pair i and C_A is a fractional concentration of acceptors. Taking into account the crystallographic structure of YAG, the lattice sum calculations

were performed in the 12.5 Å radius sphere of influence, which includes 120 ion sites. The calculated $X = 2.8 \times 10^2\ s^{-1}$ value is in good agreement with that measured in 1 at.% Nd^{3+} sample, quenching rate of $X = 2.65 \times 10^2\ s^{-1}$. This also suggests that short-range interactions of the multipolar or superexchange type are not active, contrary to arguments presented in Ref. 25.

As could be seen from Figure 4, the slope dependence of X on Nd^{3+} concentration is nearly linear up to about 1.5 at.%. Above this concentration, the quenching rate depends quadratically on ion concentration. The decay curves in 3 and 6 at.% Nd^{3+}-doped YAG could be interpreted in terms of the intermediate regime between the absence of diffusion and the rapid donor–donor transfer limits.[26] In this case, the decay is exponential only at long times with the rate calculated by Huber,[27] which shows a quadratic concentration dependence in the limit of slow migration. Nonexponential character of decays in the presence of diffusion is also consistent with results of Merkle and Powell[28] and Devor and Shazer[29] who observed energy migration to Nd^{3+} ions in some perturbed lattice sites. This was also confirmed by Diaz-Torres et al.[30] who interpreted quenching in Nd:YAG in terms of resonant energy transfer to quenching centers formed by perturbed neodymium ions. Their model predicts quadratic dependence of the energy transfer rate on concentration. Similar behavior, that is, linear quenching for low, up to about 1 at.% of Nd^{3+}, concentration and quadratic dependence for higher concentrations, has been very recently reported by Merkle et al.[31] for fine-grained Nd:YAG ceramics. The linear behavior is consistent with the quenching by direct cross-relaxation, and quadratic behavior is consistent with the picture of energy migration to sinks consisting of cross-relaxing Nd pairs at higher concentration.

Under high excitation densities, there are also efficient internal pair energy transfer upconversion processes involving two Nd^{3+}, of the type $^4F_{3/2} + {}^4F_{3/2} \rightarrow {}^4I_{11/2} + {}^2G_{9/2} \rightarrow {}^4I_{9/2} + {}^4F_{3/2}$[9] The ET (energy transfer) upconversion process reduces the population of the $^4F_{3/2}$ state and causes a lifetime shortening. Decays of the $^4F_{3/2}$ fluorescence exhibit shortening and the nonexponentiality of the decays with the increase of pumping. For high excitation density, both upconversion and downconversion compete in the de-excitation of the $^4F_{3/2}$ state.

Yb:YAG

Because of the simple electronic structure of Yb^{3+} ion, which consists of only two levels $^2F_{7/2}$ and $^2F_{5/2}$ split by spin-orbit interaction, such unfavorable processes like excited state absorption, upconversion, or cross-relaxation are not active. However, in the Yb^{3+} systems, ion–ion interaction could result in a cooperative emission.[32,33] When Yb^{3+} ion pair is excited, it undergoes cooperative upconversion yielding emission in the blue-green spectral region from the doubly excited $[^2F_{5/2} - {}^2F_{5/2}]$ pair state. According to Dexter's[34] model, cooperative transitions are due to the perturbation for

the electric transitions induced by the Coulomb interaction between two electrons on each ion, which produces transition probability for the forbidden cooperative process. As this process is strongly interionic distance dependent, it has been used as a probe for RE^{3+} ion clustering in glasses and crystals.[35,36] In our recent work, we reported on cooperative emission in the Yb^{3+}:YAG planar waveguide at room temperature.[37] Here we present new results on studying the ion–ion interaction in Yb^{3+}:YAG waveguides with different Yb^{3+} content. Observation of ytterbium pairing within YAG matrix is reported. From the analysis of the YAG lattice, it results that the first, fourfold coordinated and the second, eight fold coordinated, neighbor pairs are separated by 3.67 Å and 5.62 Å and under the assumption of electric dipole–dipole interaction should be responsible for 78% and 12% of the cooperative emission signal, respectively.

Cooperative emission spectrum of Yb:YAG/YAG structure after IR excitation at 940 nm is shown in Figure 5. Maximum of this emission is centered at 484 nm. The dependence of the cooperative emission intensity I_{coop} on excitation power and Yb^{3+} concentration was determined and is plotted in Figure 6. As observed in the log-log plots in Figure 6, I_{coop} represents a quadratic function of both excitation power and dopant concentration up to highest concentration studied of 15 at.% Yb^{3+}. This behavior is consistent with a two-ion process.

To confirm Yb^{3+} ion pairing within the YAG matrix, the high-resolution excitation spectra of the IR and visible emissions were registered at low temperature around the lowest Stark component of the $^2F_{5/2}$ level at 10,321 cm^{-1} (Fig. 7). Wavelength of a Ti:sapphire laser was scanned through the $^2F_{7/2}(0) \rightarrow {}^2F_{5/2}(1)$ transition when nonresonant $^2F_{5/2}(1) \rightarrow {}^2F_{7/2}(3)$ infrared emission at 1030 nm and cooperative blue emission at 512 nm were registered simultaneously. For comparison, absorption spectrum of a single $Yb_3Al_5O_{12}$ (YbAG) crystal is also presented. Low-temperature absorption for 15 at.%

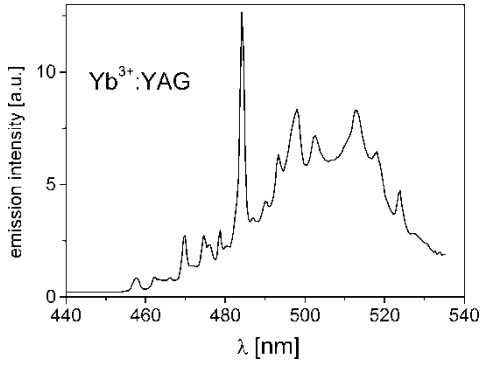

Figure 5. Cooperative emission spectrum of Yb^{3+}:YAG/YAG structure after IR excitation at 940 nm.

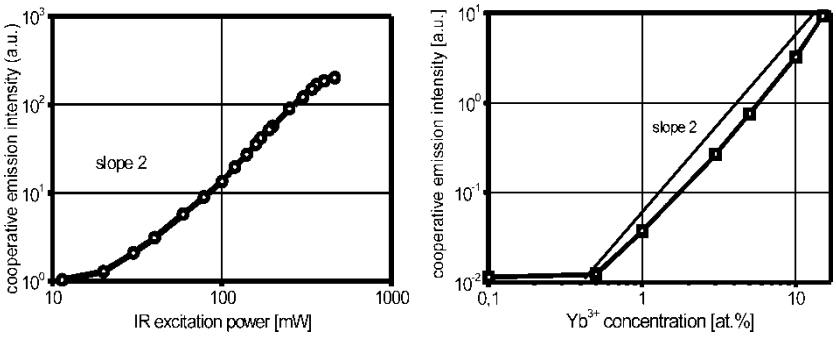

Figure 6. Dependence of the cooperative emission intensity I_{coop} on excitation power and Yb^{3+} concentration in YAG waveguides.

Yb:YAG film was measured, however the ytterbium pair lines were below the detection limit. As can be seen from Figure 7 the half-widths of the Yb^{3+} transition in YAG are greater than for other RE^{3+} ions. This is consistent with the reported observations of strong ion–lattice and ion–ion coupling for Yb^{3+} ions. In Figure 7, the sharpest lines are those corresponding with the least distorted crystal lattice of pure YbAG. The change in the Yb^{3+} concentration results in an inhomogeneous line broadening, from 10 cm^{-1} to about 18 cm^{-1} in the highly perturbed lattice with $x = 0.15$. From the comparison of the excitation spectra of the IR and cooperative emission, it is shown that IR fluorescence results mainly from the central part of the excitation profile when strongly asymmetric line profile can be observed in the case of cooperative luminescence excitation. An important part of the cooperative emission intensity results from excitation on the lower energy side, at about 10,315 cm^{-1}, of the

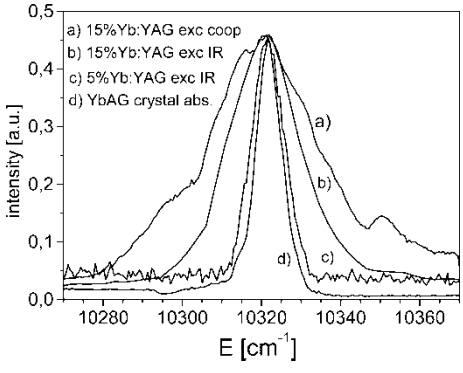

Figure 7. High-resolution excitation spectra of the IR and visible emissions registered at low temperature around the lowest Stark component of the $^2F_{5/2}$ level at 10,321 cm^{-1} in 5 and 15 at.% Yb^{3+}-doped YAG waveguides and absorption spectrum of YbAG at 10 K.

main line. However, it can be observed that excitation on both sides also on the far wings of the main line enhances cooperative emission intensity, suggesting ensembles of Yb^{3+} ions in near lattice sites including triads of ions, observed by Lupei [14,24] in RE^{3+} garnets, and Yb^{3+} ions in distorted lattice sites. For this site, which energy corresponds also with the small peak on the IR excitation profile in the 5 at.% sample, coupling between the Yb^{3+} is strong and cooperative emission is enhanced. This, together with the distance from the line center of 5 cm^{-1} (see also Fig. 2), suggests its first neighbor pair origin. Because, as mentioned earlier, the electron–phonon coupling in ytterbium is one of the strongest in the lanthanide series, the absorption and excitation lines are strongly broadened and the spectral resolution is partially lost, preventing unambiguous attribution of the spectroscopic features, especially pair-transitions.

The use of the rate equations allows us to connect the experimental results of the cooperative emission intensity with the microscopic interaction parameters. In describing the cooperative emission process between two interacting Yb^{3+} ions, a key parameter is the cooperative emission rate, which is the probability of the cooperative de-excitation of a given Yb^{3+} ion pair. An average cooperative rate X, under the assumption of weak cooperative emission, that is $X \ll W$ where W is the pump rate can be written as[38]

$$X = 2\frac{I_{coop}}{I_{IR}}\frac{1}{W\tau_2^2}$$

where τ_2 is the lifetime of the $^2F_{5/2}$ state of Yb^{3+}, and I_{coop} and I_{IR} are the cooperative and infrared emission intensities, respectively. The determined here values of 0.17 and 0.29 s^{-1} respectively for 10% and 15% doped samples are in reasonable agreement with the experimental cooperative rates of 0.13 s^{-1} reported for Yb^{3+}:$CsCdBr_3$[38] and the value of 0.37 s^{-1} found in Yb^{3+} activated $Gd_3Ga_5O_{12}$ crystal.[39]

The cooperative emission rate for a particular ion-pair can next be evaluated with the knowledge of the interionic distances and assuming identity of Yb^{3+} ions including that the ytterbium cross sections are independent on ion–ion coupling and the type of interaction. However, according to recently presented theoretical treatment of the cooperative transition probabilities for Yb^{3+} ion pairs in YAG,[40] an interionic distance between Yb^{3+} ions is not the primary factor for determining the cooperative transition probability in the crystal. As proved, the use of $(Yb_2O_{14})^{22-}$ dimmer cluster model in YAG reproduced best the experimental results indicating the necessity of taking into account the nature of chemical bonding.

Nd + Yb:YAG

Nd^{3+} and Yb^{3+} codoped crystals and glasses are extensively studied as candidates for efficient lasers. Nonradiative energy transfer from Nd^{3+} to Yb^{3+}

leads to broad-band Yb^{3+} emission, ranging from 950 to 1100 nm, after diode pumping of the Nd^{3+} ions at 810 nm. Yb + Nd:YAG waveguide lasers are considered as candidates for PDFA (praseodymium doped fiber amplifier) pump.[41,42] In our study, we employed LPE to grow, from a supersaturated molten garnet-flux high-temperature solution, $Y_{3-x-y-t}Nd_xYb_yLu_tAl_{5-z}Ga_zO_{12}$ waveguides layers on <111> oriented YAG substrates. Recently, some of us observed laser action at 1030 nm after diode laser pumping at 808 nm, as a result of efficient energy transfer from Nd^{3+} to Yb^{3+}, with the threshold of about 420 mW.[43,44]

Efficiency of the $Nd^{3+} \rightarrow Yb^{3+}$ energy transfer was investigated by comparing the ratio of the $^4I_{5/2}Yb^{3+}$ fluorescence intensity to that of the $^4F_{3/2}$ of Nd^{3+}. I_{Yb}/I_{Nd} as a function of the Yb^{3+} concentration, for a fixed neodymium content of 1 at.%, is shown in Figure 8. An onset of decrease in the intensity ratio is observed for Yb^{3+} content above 3 at.%, which could be due to increasing role of $Yb^{3+} \rightarrow Nd^{3+}$ back-transfer. Also, when the concentration of Yb^{3+} increases, a reduction of the neodymium $^4F_{3/2}$ lifetime is observed; efficiency of the energy transfer, given by $\eta = 1 - \tau/\tau_{Nd}$, where τ_{Nd} is the $^4F_{3/2}$ lifetime in the absence of Yb^{3+} ions, is plotted in Figure 8. Efficiency of the energy transfer of 88%, determined for 3 at.% Yb^{3+}+1 at.% Nd^{3+}:YAG, is higher than the efficiencies of 55–60% found for doubly doped fluoroindogallate[45] and metaphosphate[46] glasses, making YAG system of special relevance for future applications as a tunable laser gain medium. Room-temperature $Nd^{3+} \rightarrow Yb^{3+}$ energy transfer efficiencies of the order 90% have also been recently demonstrated in YAB crystals.[47]

It was observed that strong excitation of the Nd^{3+} ions at 808 nm resulted also in an intense blue-green emission from Nd + Yb activated YAG waveguides. Figure 9 shows the upconversion luminescence in two $Nd^{3+} + Yb^{3+}$: YAG structures of different activators concentration. The blue part of the

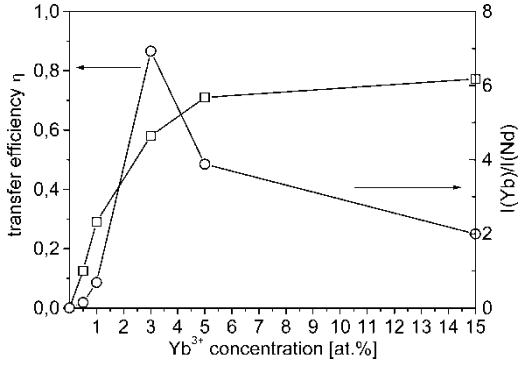

Figure 8. Efficiency of the $Nd^{3+} \rightarrow Yb^{3+}$ energy transfer in the (1 at.% $Nd^{3+} + x$ at.% Yb^{3+}):YAG waveguides and the ratio of the $^2F_{5/2}$ Yb^{3+} to $^4F_{3/2}$ Nd^{3+} emission intensities as a function of Yb^{3+} concentration.

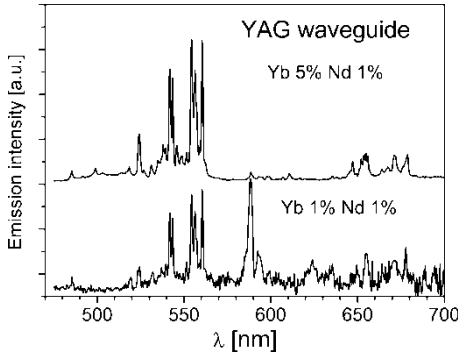

Figure 9. Visible emission spectra of $Nd^{3+} + Yb^{3+}$:YAG waveguides after selective infrared excitation of Nd^{3+} ions at 808 nm; T = 300 K

spectrum results from the cooperative emission of Yb^{3+} pairs[37] (see Fig. 5). Intense emission centered at 550 nm has been also observed by Xu et al.[48] in Yb^{3+}:YAG and ascribed to the presence of trace impurities like Er^{3+}, Tm^{3+}, or Ho^{3+} ions. However, some of the observed emission lines correspond well with transitions from the higher excited states of Nd^{3+}:YAG,[49–51] which can be excited by various, complicated ESA or ETU processes including cooperative sensitization mechanism.

The losses for the $Nd^{3+} \rightarrow Yb^{3+}$ processes are related to the back $Yb^{3+} \rightarrow Nd^{3+}$ transfer, which is nonresonant and is generally more probable in high-phonon energy matrices. Excitation at Yb^{3+} absorption wavelength at 960 nm results in an energy transfer to nearby Nd^{3+} ions and emission from the $^4F_{3/2}$ level. As shown in Figure 10, decays of the $^4F_{3/2}$ emission are characterized by the initial rise time, of the order 1.5 μs, followed, at long times, by nearly exponential decays with time constants that are much

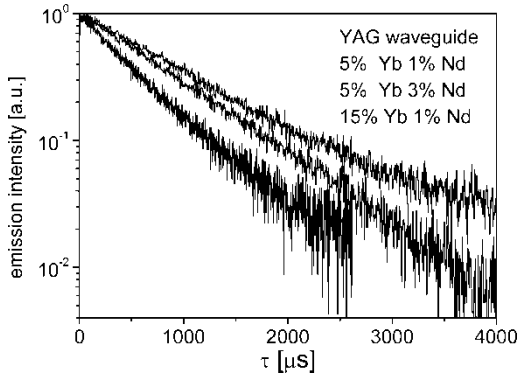

Figure 10. Decays curves of the $^4F_{3/2}$ emission in Nd + Yb:YAG waveguides after selective excitation of Yb^{3+} ions at 960 nm; T = 300 K.

longer than in the case of direct neodymium excitation. These time constants are close to the Yb^{3+} excited $^2F_{5/2}$ state lifetime. As shown in Ref. 51 for the $Nd^{3+} + Yb^{3+}$:YAG nanoceramics, the energy of the excited $^2F_{5/2}$ state of Yb^{3+} may be transferred quasi-resonantly, with the energy mismatch of $\Delta E = 24\ cm^{-1}$, to the $^4F_{3/2}$ of Nd^{3+} only when this ion is in the highest Stark level of the ground $^4I_{9/2}$ state resulting in strong temperature dependence of this process. This also explains observed decrease in the effectiveness of $Nd^{3+} \rightarrow Yb^{3+}$ energy-transfer probability above a few hundred Centigrade.

Pr:YAG

Trivalent praseodymium ion (Pr^{3+}), emitting in the UV, visible, and IR spectral ranges, is one of the most promising activators for laser, scintillator, and luminophore materials. However, most of the experimental data on Pr^{3+}:YAG available up-to-date referred to relatively lightly doped, bulk materials. The unique set of samples investigated in this work was characterized by high (up to 6 at.%) level of dopant concentration, enabling more detailed spectroscopic studies. The main aim of these studies was to examine concentration effects on the $^3P_0$ emitting level.

After short wavelength excitation into the $^3P_1$ level of Pr^{3+} ion in YAG waveguides, simultaneous emission from $^3P_0$ and $^1D_2$ excited states[53] occurs. It was observed that with the increasing Pr^{3+} concentration, the intensity of lines attributed to the $^1D_2$ emission centered around 610 and 635 nm decreases with respect to the intensity of the $^3P_0$ emission as shown in Figure 11. This suggests different magnitude of the concentration quenching and/or reabsorption processes for these levels.

Fluorescence dynamics of the $^3P_0$ and $^1D_2$ emitting levels was investigated as a function of Pr^{3+} concentration under resonant, direct excitation.

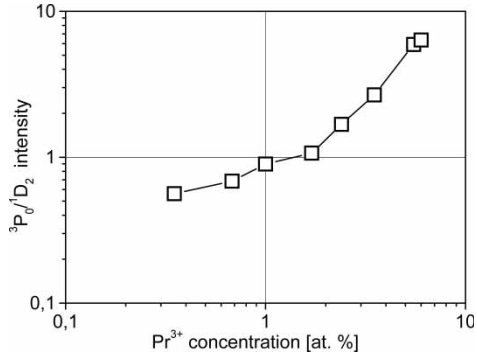

Figure 11. Ratio of the $^1D_2$ to $^3P_0$ emission intensities in Pr^{3+}:YAG waveguides as a function of Pr^{3+} concentration.

The $^1D_2$ decays were also measured after excitation into the $^3P_0$ level, and the decays of the $^3P_0$ level were obtained under two-photon upconversion excitation into the $^1D_2$ level. For both $^3P_0$ and $^1D_2$ levels, it was observed that, as the concentration of Pr^{3+} ions was increased, the fluorescence decays shortened and started being nonexponential. Using Eq. (1), the effective lifetimes τ_{eff} were calculated and are presented as a function of concentration in Figure 12. These variations of fluorescence decays with concentration indicate the presence of energy transfer processes at concentrations higher than about 0.5 at.% of Pr^{3+}. As in other Pr^{3+} investigated systems,[54] the $^1D_2$ emission is affected more strongly by quenching than the $^3P_0$ one. The effective lifetime of the $^1D_2$ state decreases from 190 μs in 0.35 at.% doped sample to about 5 μs in strongly 6 at.% doped Pr:YAG waveguide.

The $^3P_0$ emission of praseodymium can be quenched by multiphonon relaxation, cross-relaxation, and upconversion, where the latter two processes are concentration dependent. In Pr^{3+}:YAG films, after excitation of the $^3P_0$ level, emission originating from the $^1D_2$ level is clearly observed. This means that part of the $^3P_0$ excitation relaxes to $^1D_2$. As these multiplets are separated by 3328 cm^{-1},[53] the probability of multiphonon decay is not significant, and on the basis of energy gap law it is estimated to be $W_{NR} = 10{,}642\ s^{-1}$. So, it is concluded that upconversion energy transfer process is responsible for populating the $^1D_2$ level. This is also confirmed by observations, after $^3P_0$ level excitation, of the rise time in the decays of the $^1D_2$ level that exhibits clear concentration dependence, shown in Figure 13, and varies from about 0.5 to 4 μs.

From the energy levels of Pr^{3+}:YAG, it results that the more probable cross-relaxation between pairs of Pr^{3+} ion process is $^3P_0 \rightarrow {}^3H_6 = {}^3H_4 \rightarrow {}^1D_2$, which is related to the emission of 171 cm^{-1} phonon. This is confirmed by the observation of the initial rise time in the $^1D_2$ fluorescence reflecting the $^3P_0$-decay time. It should be noted that, according to the

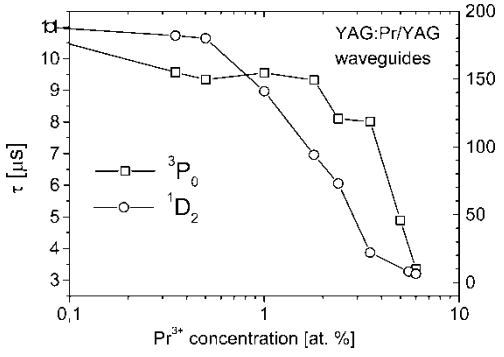

Figure 12. Concentration dependence of the effective fluorescence lifetimes of the $^3P_0$ and $^1D_2$ emissions of Pr^{3+}-activated YAG waveguides.

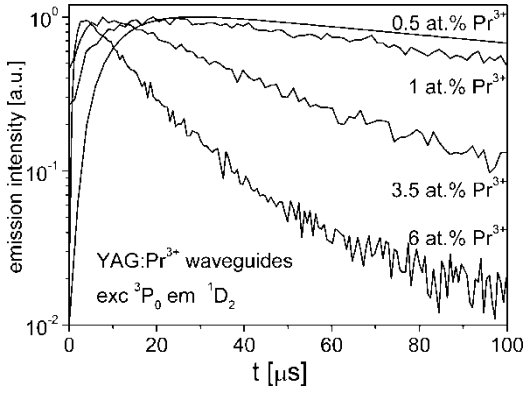

Figure 13. Time evolution of the $^1D_2$ emissions after $^3P_0$ level excitation in Pr^{3+}: YAG waveguides with different activator concentrations.

solution of the rate equations,[55,56] the rise time of $^1D_2$ emission is governed by the lifetime of the $^3P_0$ state, followed by an exponential decay faster than half the intrinsic decay time. Our measurements indicated a rise time that was much shorter than the $^3P_0$-decay time for a given concentration. The equivalent situation in LaF_3:Pr^{3+} has been explained in Ref. 56 as being due to the limitations of the assumed model, that is, in the concentrated Pr^{3+} systems, decays are no longer exponential, and quenching rates could be different for the specific ion pairs.

In order to evaluate the rates of $^3P_0$ quenching via cross-relaxation, the formalism describing fluorescence dynamics behavior in the presence of traps proposed by Huber in Ref. 57 was used. It was shown that function describing the decay of donor excitation in the presence of only one type of acceptors and the absence of donor–donor and back transfer is given by

$$f(t) = e^{-t/\tau_0} \times \prod_n (1 - c_A + c_A e^{-X_{0n}t}) \tag{3}$$

where c_A represents the concentration of acceptors, X_{0n} the trapping rate between a donor at site 0 and an acceptor at site n, and $\prod$ denotes the product over all the lattice sites. X_{0n} can be related to trapping rate of the nearest neighbor by $X_{0n} = X_{01}(R_{01}/R_{0n})^s$, where R_{0n} denotes the distance between site 0-n pair, and s stands for interaction type being equal to 6, 8, 10 for dipole–dipole, dipole–quadrupole, and quadrupole–quadrupole interactions, respectively. Using this formalism, the nearest-neighbor trapping rates X_{01} were determined by fitting the directly excited $^3P_0$ decays with Eq. (3) as shown in Figure 14. Best fit was obtained for a sphere of interaction of 3 Å radius; its further increasing did not affect the fitting curves. For the most concentrated sample, the nearest neighbor quenching rate was found to be $2.37 \times 10^6\ s^{-1}$ and is close to the values of $2.65 \times 10^6\ s^{-1}$ and

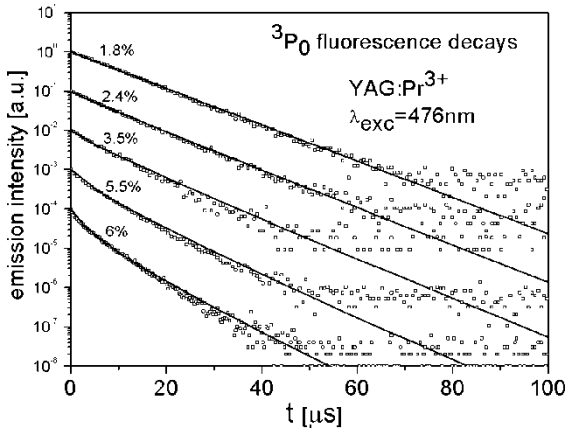

Figure 14. The concentration-dependent decay patterns of the luminescence from the $^3P_0$ level of Pr^{3+}:YAG; solid curves are numerical simulations with Eq. (3).

$2.82 \times 10^6\ s^{-1}$ reported by Wu et al. [58] for concentrations of 1% and 2% respectively.

The next step in our investigation was to determine the total cross-relaxation rates defined as $X = 1/\tau_{eff} - 1/\tau_0$, where τ_{eff} is the effective fluorescence decay time [see Eq. (1)] and τ_0 is the isolated ion lifetime measured in the low-concentration sample. For the most concentrated sample, we obtained $X_P(6\%\text{Pr:YAG}) = 1.2 \times 10^6\ s^{-1}$. Using Eq. (2), with the determined above $X_{01} = 2.37 \times 10^6\ s^{-1}$, we obtained $X = 7.3 \times 10^5\ s^{-1}$, which is somewhat lower than X_P indicating that other than assumed cross-relaxation processes are also active in de-excitation of the $^3P_0$ state. Additional concentration-dependent quenching channel for the $^3P_0$ level that should be taken into account is the upconversion by energy transfer[59] or excited state absorption[60,61] to the $4f5d$ praseodymium levels resulting in the UV emission.[60]

High-resolution excitation measurements have been performed at low temperature in the vicinity of the $^3P_0$ absorption at 20,538 cm^{-1}. Figure 15 shows the Pr^{3+} excitation spectra, obtained by scanning the dye laser across the $^3H_4(1) \rightarrow {}^3P_0$ absorption line and detecting the $^3P_0 \rightarrow {}^3H_6$ fluorescence, in Pr:YAG waveguide samples of 0.5 and 6 at.% concentrations. It could be seen that the character of the spectra changes with concentration. In the diluted YAG:0.5 at.% Pr^{3+} sample, regular ion transition at 20,538 cm^{-1} dominates; weak peaks observed on either side of the main line are attributed to Pr^{3+} ions in other than D_2 sites or to ion clusters. In the 6 at.% Pr^{3+}:YAG waveguide, the excitation line became much broader and strong additional transitions appear; the spectrum of these minority lines extends in 6 at.% Pr^{3+}:YAG over 40 cm^{-1}, indicating important crystal-field distortion and high degree of lattice strain.

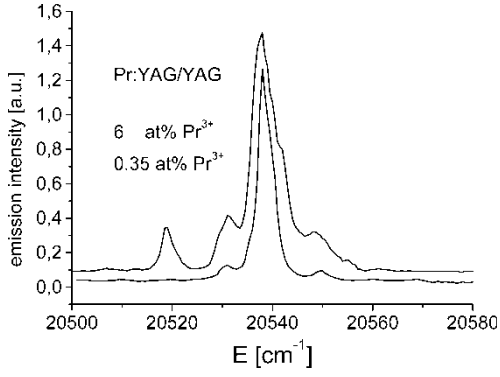

Figure 15. Excitation spectra in the vicinity of the $^3P_0$ absorption at 20,538 cm^{-1}, obtained by scanning the dye laser across the $^3H_4(1) \rightarrow {}^3P_0$ absorption line and detecting the $^3P_0 \rightarrow {}^3H_6$ fluorescence, in 0.5 and 6 at.% Pr^{3+}:YAG waveguides.

Quenching of the praseodymium $^1D_2$ emission is due to the quasi-resonant or phonon-assisted (less than 100 cm^{-1} phonons) cross-relaxation process, which is attributed to the following transitions between two ions: $^1D_2(1) \rightarrow {}^1G_4(1-5) = {}^3H_4(1) \rightarrow {}^3F_3(1-4)$.[38] It is also known that two $^1D_2$ ions that which couple between themselves can undergo an upconversion process of the type $^1D_2(1) + {}^1D_2(1) \rightarrow {}^3P_2(\text{l-}5) + {}^1G_4(8, 9)$, which leads to anti-Stokes $^3P_0$ emission. With excitation in the $^1D_2$ level, we observed intense upconverted emission from the $^3P_0$ level and also weak UV fluorescence from the $4f5d$ band. The total quenching rate of the $^1D_2$ emission, for the most concentrated sample, was found to be $X_D(6\%\text{Pr:YAG}) = 1.5 \times 10^5\ s^{-1}$, which, by using Eq. (2), gives the nearest neighbor quenching rate of $X_{D01} = 3.5 \times 10^5\ s^{-1}$, which is lower than our earlier calculations based on ion-pair measurements.[62]

The presented results show the complexity of the processes responsible for the quenching of emissions in Pr^{3+}:YAG at high dopant concentrations, both $^3P_0$ and $^1D_2$ emitting levels are coupled by various energy transfer processes, including processes engaging low-lying, at about 33,000 cm^{-1}, $4f^{n-1}\ 5d$ levels.

CONCLUSIONS

In this work, we have examined the concentration-dependent mechanisms that determine luminescence properties of Nd^{3+}, Yb^{3+}, and Pr^{3+} doped YAG waveguides that were grown using liquid phase epitaxy technique. The high concentration of activator, which is favorable for operation of planar waveguide devices and waveguide effect itself, results in high optical intensities within the small volume that increase the probability of

neighboring ions being simultaneously excited. Under pulsed excitation, dynamic studies of different energy transfer mechanisms active in the investigated systems were performed, and values of concentration-dependent energy transfer rates were established. The use of high-resolution laser spectroscopy at low temperature allowed investigation of the inhomogeneous line profiles. Ion pairing in the investigated systems has been confirmed by analysis of the cooperative emission excitation spectra and selectively excited fluorescence dynamics respectively in Yb^{3+}:YAG/YAG and Nd^{3+}:YAG/YAG planar waveguides. This study confirmed that RE^{3+} doped YAG waveguides grown by LPE have no additional structural defects, reflecting its high quality.

ACKNOWLEDGMENTS

This work was supported by the Polish Ministry of Education and Science under KBN grants 3T11B02627 and 3T11B00327.

REFERENCES

1. Ferrand, B.; Pelenc, D.; Chartier, I.; Wyon, Ch. Growth by LPE of Nd:YAG single crystal layers for waveguide laser applications. *J. Cryst. Growth* **1993**, *128*, 965–969.
2. Martynyuk, N. V.; Ubizskii, S. B.; Buryy, O. A.; Becker, K. D.; Kreye, M. Optical in-situ study of the oxidation and reduction kinetics of Yb-substituted YAG epitaxial films. *Phys. status solidic* **2005**, *2*, 330–333.
3. Sugimoto, N.; Ohishi, Y.; Katoh, Y.; Tate, A.; Shimokozono, M.; Sudo, S. A ytterbium- and neodymium-co-doped yttrium aluminum garnet-buried channel waveguide laser pumped at 0.81 μm. *Appl. Phys. Lett.* **1995**, *67*, 582–584.
4. Van der Ziel, J. P.; Bonner, W. A.; Kopf, L.; Singh, S.; Van Uitert, L. G. Coherent emission from Ho^{3+} ions in epitaxially grown thin aluminum garnet films. *Phys. Lett.* **1972**, *22*, 105–106.
5. Mackenzie, J. I.; Mitchell, S. C.; Beach, R. J.; Meissner, H. E.; Shepherd, D. P. A 15W diode-side-pumped Tm:YAG waveguide laser at 2 μm. *Electron. Lett.* **2001**, *37*, 898–899.
6. Zayhowski, J. J.; Mooradian, A. Single frequency microchip Nd lasers. *Opt. Lett.* **1989**, *14*, 24–26.
7. Kaminskii, A. A. *Laser Crystals*; Springer-Verlag: Berlin, 1981.
8. Hooge, F. N. Spectra of praseodymium in yttrium gallium garnet and in yttrium aluminum garnet. *J. Chem. Phys.* **1966**, *45*, 4504–4509.
9. Guy, S.; Bonner, C. L.; Shepherd, D. P.; Hanna, D. C.; Trooper, A. C.; Ferrand, B. High-inversion densities in Nd:YAG upconversion and bleaching. *IEEE J. Quantum Electronics* **1998**, *34*, 900–909.
10. Mao, Y.; Deng, P.; Gan, F. Concentration and temperature dependence of spectroscopic properties of highly-doped Nd:Yag crystal grown by temperature gradient technique (TGT). *Phys. Status solidi a* **2002**, *193*, 329–337.

11. Wu, Xingkun; Denis, W. M.; Yen, W. M. Temperature dependence of cross-relaxation processes in Pr^{3+}-doped yttrium aluminum garnet. *Phys. Rev. B* **1994**, *50*, 6589–6595.
12. Malinowski, M.; Szczepański, P.; Woliński, W.; Wolski, R.; Frukacz, Z. Inhomogeneity studies of Pr^{3+}:YAG using time resolved spectroscopy. *J. Phys, Condens. Matter* **1993**, *5*, 6469–6482.
13. Jabloński, R.; Sarnecki, J.; Mazur, K.; Sass, J.; Skwarcz, J. ESR and X-ray diffraction measurements of Nd substituted yttrium aluminum garnet films. *J. Alloy. Compd.* **2000**, *300–301*, 316–321.
14. Lupei, V. Self quenching of Nd^{3+} emission in laser garnet crystals. *Opt. Mater.* **2001**, *16*, 137–152.
15. Lupei, V.; Lupei, A.; Georgescu, S.; Diaconescu, B.; Taira, T.; Sato, Y.; Kurimura, S.; Ikesue, A. High-resolution spectroscopy and emission decay in concentrated Nd:YAG ceramics. *J. Opt. Soc. Am. B* **2002**, *19*, 360–368.
16. Singh, S.; Bonner, W. A.; Grodkiewicz, W. H.; Grosso, M.; Van Uitert, L. G. Nd-doped yttrium aluminium garnet with improved fluorescence lifetime of the $^4F_{3/2}$ state. *Appl. Phys. Lett.* **1976**, *29*, 343–345.
17. Lupei, A.; Lupei, V.; Georgescu, S.; Ionescu, C.; Yen, W. M. Mechanisms of energy transfer between Nd^{3+} ions in YAG. *J. Lumin.* **1987**, *39*, 35–43.
18. Lupei, V.; Lupei, A.; Georgescu, S.; Ionescu, C. Energy transfer between Nd^{3+} ions in YAG. *Opt. Commun.* **1986**, *60*, 59–63.
19. Krupke, W. Radiative transition probabilities within the $4f^3$ ground configuration of Nd:YAG. *IEEE J. Quantum Electronics* **1971**, *7*, 153–159.
20. Devor, P. D.; deShazer, L. G.; Pastor, R. C. Nd:YAG quantum efficiency and related radiative properties. *IEEE J. Quantum Electronics* **1989**, *25*, 1863–1873.
21. Kaminskii, Alexander A. Laser crystals. In *Springer Series in Optical Sciences*; Ivey, H. F., (ed); Springer-Verlag: New York, 1981.
22. Kushida, T.; Marcos, H. M.; Geusic, J. E. Laser transition cross section and fluorescence branching ratio for Nd^{3+} in yttrium aluminum garnet. *Phys. Rev.* **1968**, *167*, 289–291.
23. Barthem, R. B.; Buisson, R.; Vial, J. C.; Harmand, H. Optical properties of Nd^{3+} pairs in $LiYF_4$ existence of a short range interaction. *J. Lumin.* **1986**, *34*, 295–305.
24. Lupei, V.; Lupei, A. Emission dynamics of the $^4F_{3/2}$ level in Nd^{3+} YAG at low pump intensities. *Phys. Rev. B* **2000**, *61*, 8087–8097.
25. Lupei, A.; Lupei, V. RE^{3+} pairs in garnets and sesquioxides. *Opt. Mater.* **2003**, *24*, 181–189.
26. Auzel, F. Upconversion and anti-stokes processes with f and d ions in solids. *Chem. Rev.* **2004**, *104*, 139–173.
27. Huber, D. L. Dynamics of incoherent transfer. In *Laser Spectroscopy of Solids*; Yen, W. M., Selzer, R. M., (ed); Springer-Verlag: Berlin, 1981; pp. 83–111.
28. Merkle, L. D.; Powell, R. C. Energy transfer among Nd^{3+} ions in garnet crystals. *Phys. Rev. B* **1979**, *20*, 75–84.
29. Devor, P. D.; deShazer, L. G. Evidence of Nd:YAG quantum efficiency dependence on nonequivalent crystal field effects. *Optics Communications* **1983**, *46*, 97–102.
30. Diaz-Torrez, L. A.; Barbosa-Garcia, O.; Hernandez, J. M.; Pinto-Robledo, V.; Sumida, D. Evidence of energy transfer among Nd ions in Nd:YAG driven by a mixture of exchange and multipolar interactions. *Opt. Materials* **1998**, *10*, 319–326.

31. Merkle, L. D.; Dubinskii, M.; Schepler, K. L.; Hedge, S. M. Concentration quenching in fine-grained ceramic Nd:YAG. *Optics Express* **2006**, *14*, 3893–3905.
32. Nakazawa, E.; Shionoya, S. Cooperative luminescence in $YbPO_4$. *Phys. Rev. Lett.* **1970**, *25*, 1710–1712.
33. Ovsyankin, V. V. Spectroscopy of solids containing rare earth ions. In *Modern Problems in Condensed Matter Sciences*; Kaplyanskii, A. A. and Macfarlane, R. M., (ed); Elsevier Science: New York, 1987, 343.
34. Dexter, D. L. Cooperative optical absorption in solids. *Phys. Rev.* **1962**, *126*, 1962–1967.
35. Auzel, F.; Meichenin, D.; Pelle, F.; Goldner, P. Cooperative luminescence as a defining process for RE-ions clustering in glasses and crystals. *Opt. Mater.* **1994**, *4*, 35–41.
36. Montoya, E.; Bausa, L. E.; Schaudel, B.; Goldner, P. Yb^{3+} distribution in $LiNbO_3$: (MgO) studied by cooperative luminescence. *J. Chem. Phys.* **2001**, *114*, 3200–3207.
37. Malinowski, M.; Kaczkan, M.; Piramidowicz, R.; Frukacz, Z.; Sarnecki, J. Cooperative emission in Yb^{3+}:YAG planar epitaxial waveguides. *J. Lumin.* **2001**, *94–95*, 29–33.
38. Goldner, Ph.; Pellé, F.; Meichenin, D.; Auzel, F. Cooperative luminescence in ytterbium doped $CsCdBr_3$. *J. Lumin.* **1997**, *71*, 137–150.
39. Courrol, L. C.; Samad, R. C.; Madej, C. Cooperative emission in Yb doped GGG crystals. *Annals of the Brazilian Commission for Optics* **2000**, *2*, 102–104.
40. Ishii, T. First-principles calculations for the cooperative transitions of Yb^{3+} dimer clusters in $Y_3Al_5O_{12}$ and Y_2O_3. *J. Chem. Phys.* **2005**, *122*, 024705-1–024705-6.
41. Sugimoto, N.; Ohishi, Y.; Katoh, Y.; Tate, A.; Shimokozono, M.; Sudo, S. A ytterbium- and neodymium-co-doped yttrium aluminum garnet buried channel waveguide laser pumped at 0.81 μm. *Appl. Phys. Lett.* **1995**, *67*, 582–584.
42. Shimokozono, M.; Sugimoto, N.; Tate, A.; Katoh, Y.; Tanno, M.; Fukuda, S.; Ryuoh, T. Room temperature operation of an Yb-doped $Gd_3Ga_5O_{12}$ buried channel waveguide laser at 1.025 μm wavelength. *Appl. Phys. Lett.* **1996**, *68*, 2177–2179.
43. Wnuk, A.; Kopczynski, K.; Sarnecki, J.; Mlynczak, J.; Mierczyk, Z.; Malinowski, M. Interaction between Nd^{3+} and Yb^{3+} ions in epitaxial YAG laser waveguide. CE6-1-FRI, CLEO Munich: Germany, June 2005, 12–17.
44. Sarnecki, J. Technology of epitaxial garnet films for lasers. PhD thesis, ITME: Warsaw, 2006.
45. de Sousa, D. F.; Batolioto, F.; Bell, M. J.V.; Oliveira, S. L.; Nunes, L. A.O. Spectroscopy of Nd^{3+} and Yb^{3+} codoped fluoroindogallate glasses. *J. Appl. Phys.* **2001**, *90*, 3308–3313.
46. Parent, C.; Laurin, C.; Le Flem, G.; Hagenmuller, H. $Nd^{3+} \rightarrow Yb^{3+}$ energy transfer in glasses with composition close to $LiLnP_4O_{12}$ metaphosphate (Ln = La, Nd, Yb). *J. Lumin.* **1986**, *36*, 49–55.
47. Jaque, D.; Ramirez, M. O.; Bausá, L.; Speghini, A.; Bettinelli, M.; Cavalli, E. Influence of Nd^{3+} and Yb^{3+} concentration on the $Nd^{3+} \rightarrow Yb^{3+}$ energy-transfer efficiency in the $YAl_3(BO_3)_4$ nonlinear crystal: determination of optimum concentrations for laser applications. *J. Opt. Soc. Am. B* **2004**, *21*, 1203–1209.
48. Xu, X.; Zhao, Z.; Song, P.; Jiang, B.; Zhou, G.; Xu, J.; Deng, P.; Bourdet, G.; Chantaloup, J. C.; Zou, J-P.; Fulop, A. Upconversion luminescence in Yb^{3+} doped yttrium aluminum garnets. *Physica B* **2005**, *357*, 365–369.

49. Mares, J. A.; Jacquier, B.; Pedrini, C.; Boulon, G. Selective one-photon and two stepwise excitations of Nd^{3+} YAG and visible fluorescence in YAG:Nd. *Mater. Chem. Phys.* **1989**, *21*, 237–259.
50. Guyot, Y.; Manaa, H.; Rivoire, J. Y.; Moncorge, R.; Garnier, N.; Descroix, E.; Bon, M.; Laporte, P. Excited state absorption and up-conversion studies of Nd^{3+} doped single crystals $Y_3Al_5O_{12}$, $YLiF_4$ and $LaMgAl_{11}O_{19}$. *Phys. Rev. B* **1995**, *51*, 784–799.
51. Bednarkiewicz, A.; Hreniak, D.; Dereń, P.; Stręk, W. Hot emission in Nd^{3+}/Yb^{3+}:YAG nanocrystalline ceramics. *J. Lumin.* **2003**, *102–103*, 438–444.
52. Bednarkiewicz, A.; Stręk, W. Laser-induced hot emission in Nd^{3+}/Yb^{3+}:YAG nanocrystallite ceramics. *J. Phys. D: Appl. Phys.* **2002**, *35*, 2503–2507.
53. Gruber, J. B.; Hills, M. E.; Macfarlane, R. M.; Morrison, C. A.; Turner, G. A. Symmetry, selection rules, and energy levels of Pr^{3+}: $Y_3Al_5O_{12}$. *Chem. Phys.* **1989**, *134*, 241–257.
54. Balda, R.; Fernandez, J.; Saez de Ocariz, I.; Voda, M.; Garcia, A. J.; Khaidukov, N. Laser spectroscopy of Pr^{3+} ions in $LiKY_{1-x}Pr_xF_5$ single crystals. *Phys. Rev. B* **1999**, *59*, 9972–9980.
55. Joubert, M. F. Rôle de l'interaction d'échange sur les propriétés de fluorescence de matériaux concentrés en terbium. PhD thesis, Univ. Claude Bernard: Lyon, 1982.
56. Buisson, R.; Vial, J. C. Transfer inside pairs of Pr^{3+} in LaF_3 studied by up-conversion fluorescence. *J. Phys. Lett.* **1981**, *42*, L-115–118.
57. Huber, D. L. Fluorescence in the presence of traps. *Phys. Rev. B* **1979**, *20*, 2307–2314.
58. Wu, Xingkun; Denis, W. M.; Yen, W. M. Temperature dependence of cross-relaxation processes in Pr^{3+}-doped yttrium aluminum garnet. *Phys. Rev. B* **1994**, *50*, 6589–6595.
59. Anker, D. S.; Merkle, L. D. Ion–ion upconversion excitation of the 4f5d configuration in $Pr:Y_3Al_5O_{12}$ experiments and Forster theory-based rate equation model. *Appl. Phys.* **1999**, *86*, 2933–2940.
60. Ganem, J.; Denis, W. M.; Yen, W. M. One-color sequential pumping of the 4f5d bands in Pr-doped yttrium aluminum garnet. *J. Lumin.* **1992**, *54*, 79–87.
61. Nicola, S.; Descroix, E.; Joubert, M. F.; Guyot, Y.; Laroche, M.; Semashko, V. V.; Tkatchuk, A. A.; Malinowski, M. Potentiality of Pr^{3+}- and $Pr^{3+} + Ce^{3+}$—doped crystals for tuneable UV upconversion lasers. *Opt. Mater.* **2003**, *22*, 139–146.
62. Malinowski, M.; Szczepański, P.; Woliński, W.; Wolski, R.; Frukacz, Z. Inhomogeneity studies of Pr^{3+}:YAG using time resolved spectroscopy. *J. Phys. Condens. Matter* **1993**, *5*, 6469–6482.